Biosensors and Bioelectronics 78 (2016) 200–205

Contents lists available at ScienceDirect

Biosensors and Bioelectronics

journal homepage: www.elsevier.com/locate/bios

Short communication

Aptamer-based colorimetric detection of proteins using a branched DNA cascade amplification strategy and unmodified gold nanoparticles

Chia-Chen Chang [a], Chen-Yu Chen [b,c,d], Tsung-Liang Chuang [a], Tzu-Heng Wu [e], Shu-Chen Wei [f], Hongen Liao [g], Chii-Wann Lin [a,e,h,*]

[a] Institute of Biomedical Engineering, National Taiwan University, Taipei 106, Taiwan, ROC
[b] Department of Obstetrics and Gynecology, Mackay Memorial Hospital, Taipei 104, Taiwan, ROC
[c] Department of Medicine, Mackay Medical College, Taipei 252, Taiwan, ROC
[d] Mackay Junior College of Medicine, Nursing, and Management, Taipei 112, Taiwan, ROC
[e] Institute of Biomedical Electronic and Bioinformatics, National Taiwan University, Taipei 106, Taiwan, ROC
[f] Department of Internal Medicine, National Taiwan University Hospital and College of Medicine, Taipei 100, Taiwan, ROC
[g] Department of Biomedical Engineering, School of Medicine, Tsinghua University, Beijing 100084, PR China
[h] Center for Emerging Material and Advanced Devices, National Taiwan University, Taipei 106, Taiwan, ROC

ARTICLE INFO

Article history:
Received 12 August 2015
Received in revised form
15 November 2015
Accepted 17 November 2015
Available online 18 November 2015

Keywords:
Aptamer
Gold Nanoparticle
Colorimetric detection
Branched DNA cascade amplification
Vascular endothelial growth factor

ABSTRACT

A branched DNA amplification strategy was employed to design a colorimetric aptameric biosensor using unmodified gold nanoparticles (AuNPs). First, a programmed DNA dendritic nanostructure was formed using two double-stranded substrate DNAs and two single-stranded auxiliary DNAs as assembly components via a target-assisted cascade amplification reaction, and it was then captured by DNA sensing probe-stabilized AuNPs. The release of sensing probes from AuNPs led to the formation of unstable AuNPs, promoting salt-induced aggregation. By integrating the signal amplification capacity of the branched DNA cascade reaction and unmodified AuNPs as a sensing indicator, this amplified colorimetric sensing strategy allows protein detection with high sensitivity (at the femtomole level) and selectivity. The limit of detection of this approach for VEGF was lower than those of other aptamer-based detection methods. Moreover, this assay provides modification-free and enzyme-free protein detection without sophisticated instrumentation and might be generally applicable to the detection of other protein targets in the future.

© 2015 Published by Elsevier B.V.

1. Introduction

Aptamers, like antibodies, have high-affinity binding interactions toward target molecules with great specificity. Therefore, aptamers are considered alternative recognition elements to monoclonal antibodies and are used extensively as sensors and diagnostic agents (Chang et al., 2011; Kim et al., 2014; Ma et al., 2015). A number of aptamer-based sensing systems, so-called aptasensors, have been reported, including electrochemistry (Xie et al., 2014), surface plasmon resonance (Chang et al., 2012b), fluorescence systems (Zhao et al., 2014), colorimetric assays (Chang et al., 2014a), and quartz crystal microbalance (Song et al., 2014). Despite the attractive sensitivity of these methods, most require the immobilization of DNA aptamers on the sensing surface or fluorescence labeling, which are usually laborious and time-consuming. In addition, the expensive synthesis of thiol-modified or fluorescence-labeled probes increases the cost of detection. As an alternative approach toward the development of label-free and immobilization-free aptasensors, unmodified gold nanoparticle (AuNP)-based colorimetric strategies have received intensive attention during the last 10 years owing to their simplicity and ease of operation (Li and Rothberg, 2004). This colorimetric sensing method takes advantage of the red-to-blue color change that arises from surface plasmon coupling during AuNP aggregation and can readily be seen by the naked eye (Saha et al., 2012). Typically, AuNPs were originally stabilized with unstructured target-binding aptamers. Upon binding to their target, aptamers fold into unique structures that switch off from AuNP surfaces, resulting in AuNP aggregation (Liu, 2012). Recently, we developed a signal-on architecture for aptamer-based sensors via a target-induced structure-switching DNA aptamer (Chang et al., 2013, 2014b). Although these colorimetric approaches are simple, their sensitivity is still unsatisfactory. A major limitation of previous label-free AuNP sensors is that each target interacts with only a single DNA probe on AuNP surfaces, thus hindering the

* Corresponding author at: Center for Emerging Material and Advanced Devices, National Taiwan University, Taipei 106, Taiwan, ROC.
E-mail address: cwlinx@ntu.edu.tw (C.-W. Lin).

http://dx.doi.org/10.1016/j.bios.2015.11.051
0956-5663/© 2015 Published by Elsevier B.V.

sensing performance. As such, a simple and straightforward amplified approach for label-free AuNP-based aptasensing still needs to be developed.

Recently, interest in isothermal nucleic acid amplification has grown as an efficient way to amplify biosensing events (Chang et al., 2012a; Jung and Ellington, 2014; Li and Macdonald, 2015). Various approaches, including enzyme-assisted signal amplification strategies and enzyme-free signal cascades, have been employed for DNA or other targets using aptamers as the molecular recognition unit (Wang et al., 2014). Among the signal amplification methods, hybridization chain reaction (HCR), in which one target molecule leads to a chain reaction of recognition and hybridization events between a pair of complementary, kinetically trapped hairpins, has attracted considerable attention (Huang et al., 2011). A prominent merit of HCR over other competing amplification assays is that it allows for specific self-assembly and extension at room temperature without the involvement of enzymes. Nevertheless, unlike exponential amplification methods, such as polymerase chain reaction, the current form of HCR provides linear DNA self-assembly reaction kinetics (Dirks and Pierce, 2004). In addition, the reaction is slow; several hours are required to obtain the final signal, which is unfavorable for point-of-care diagnostics (Spiga et al., 2014; Wang et al., 2015). Lately, Xuan and Hsing (2014) developed a nonlinear HCR (NLHCR) system that provides exponential growth of branched DNA nanostructures after initiation via the DNA trigger. It has distinct advantages over the conventional HCR procedure, including a higher amplification efficiency and more rapid amplification kinetics. Although this approach is designed for DNA sensing within 30 min, it is expensive to modify single-stranded DNA with fluorophores. Additionally, its application is currently limited to nucleic acid analysis and it has not been validated as a signal amplification strategy for the design of AuNP-based colorimetric biosensors.

Herein, a label-free colorimetric aptasensor system was developed and integrated with the NLHCR strategy to achieve a sensitive protein assay. Vascular endothelial growth factor (VEGF), an important protein for angiogenesis and vascular permeabilization, was selected as a model protein (Otrock et al., 2007). By using this colorimetric assay, as few as 3.7 fmole of VEGF could be detected within an hour.

2. Experimental

2.1. Colorimetric assay using citrate-capped AuNPs

Prior to measurements, S1 and S2 were formed separately by heating mixtures of equimolar solutions (4 μM) of the a strand and b strand for 5 min and cooling to room temperature for 1 h before use. In the first step, target proteins were mixed with aptamer hairpin probes in phosphate-buffered saline (PBS) buffer solution (40 μL) and then incubated for 10 min (solution A). Afterward, equimolar solutions (4 μM) of S1, S2, A1, and A2 were added to the mixture solution (protein/hairpin probe) (solution B). After incubation for 25 min, 50 μL of solution B was added to an AuNP solution of 150 μL (solution C). After 10 min, solution C was monitored by UV–vis characterization.

2.2. Colorimetric assay using DNA sensing probe-stabilized AuNPs

First, solution A and solution B were prepared as previously described. Simultaneously, 10 μL of 6 μM DNA sensing probe was added to 140 μL of AuNP solution (solution D). After incubation of solution B for 25 min, 50 μL of solution B was added to 150 μL of solution D (solution E). Next, solution E was reacted for 10 min and 1 μL of NaCl (2 M) was added to the reaction mixture for 5 min.

For other details please see Supplementary materials.

3. Results and discussion

3.1. Colorimetric assay using citrate-capped AuNPs

The principle of the branched DNA cascade amplification-based aptamer detection method is illustrated in Scheme 1. This approach consists of five main components: a bifunctional hairpin probe (HP in Scheme 1), two double-stranded substrate DNAs (S1 and S2), and two single-stranded auxiliary DNAs (A1 and A2). The bifunctional hairpin probe consists of the VEGF aptamer sequence (blue) and the initiation sequence to trigger the NLHCR amplification reaction (yellow). Part of the initiation sequence is specially designed to be complementary to the VEGF binding aptamer sequence in an initially locked format. This probe is employed as a bridge to connect the aptamer sensing module and the NLHCR amplification module. In the absence of VEGF, the aptamer probe exists predominantly as a hairpin-folded structure at equilibrium, and the amplification reaction does not occur; it is 'closed' for NLHCR. Unlike traditional double-stranded DNAs with a duplex structure, the substrate DNAs with a single-stranded toehold domain (5 nucleotide (nt); strand a for S1 and S2) are designed to have the unpaired domains in the middle, which result in bulge-loop structures. To avoid spontaneous opening of substrate DNAs ascribed to the breath of each end of the substrates (Jiang et al., 2014), the bulged loop sequences of S1 and S2 were both designed to have 7 nt longer than the toehold domain. Additionally, auxiliary DNAs are designed to have no additional secondary structure because the presence of secondary structure in the single-stranded auxiliary DNAs could slow the process of DNA branch migration exceedingly (Zhang and Seelig, 2011). Predicted secondary structures of S1, S2, and HP were examined using NUPACK in Fig. S1. Thus, the substrate DNAs and hairpin probe stay metastable and can coexist with auxiliary DNAs until triggered by protein targets.

After the addition of AuNPs, single-stranded DNA (A1 and A2) is adsorbed by citrate-capped AuNPs and the stability of AuNPs increases, resulting in AuNP dispersion. In the presence of VEGF, it binds to the corresponding aptamer sequence and disturbs intramolecular DNA hybridization to open the hairpin structure. Therefore, conformation rearrangement of the hairpin aptamer probe results in a switch to the 'activated' initiation sequence, and thereby acts as a trigger for a cascade amplification reaction of NLHCR. In the initial step of NLHCR, partial strand displacement of S1 is initiated by toehold hybridization with the initiation sequence of the aptamer probe on the S1a strand and occurs via the migration of the initiation sequence at the 5' end. Then, A1 binds to the newly exposed toehold domain of the S1b strand, and the double-stranded byproduct B1 is released from S1. The brown domain of S2a serves as a toehold for interactions with the unstructured region of S1a, resulting in the formation of a two-branch DNA structure. After the introduction of A2, the two-branch DNA is separated to release the byproduct B2 via A2-assisted strand displacement reactions. Additionally, A2 provides two new initiation sequences to which S1 binds to initiate a new cycle of the amplification reaction. Therefore, dendrimer-like DNA is continuously constructed by the chain reaction. After incubation with the AuNP solution, the steric hindrance and complex conformation of dsDNA (Hussain et al., 2013; Shawky et al., 2010) result in ineffective adsorption of the DNA dendrimer on AuNPs, which makes AuNPs susceptible to salt-induced aggregation. In the absence of VEGF, DNA amplification components (i.e., substrate DNA and auxiliary DNA) exist stably so that nearly no amplification is triggered. Accordingly, auxiliary DNA in its single-stranded form can render the AuNPs stable against color changes.

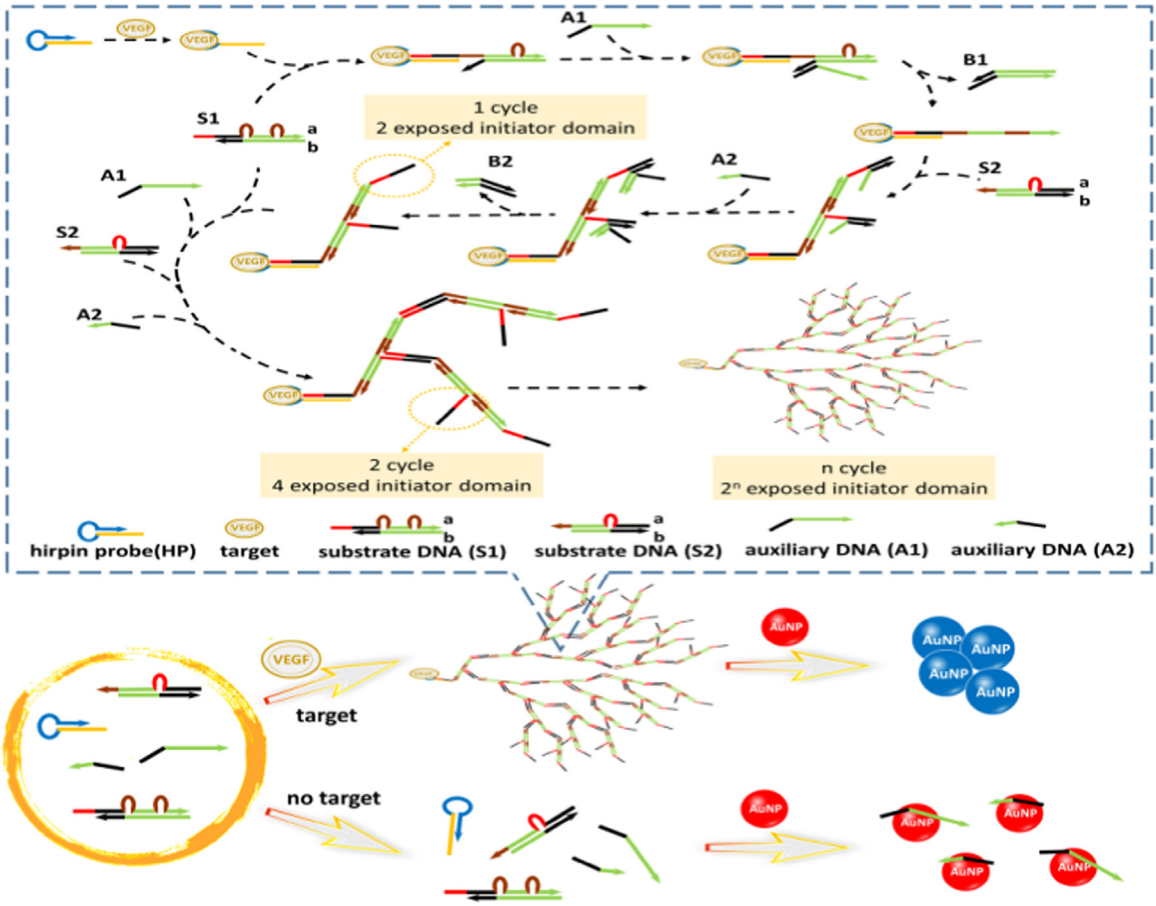

Scheme 1. Schematic illustration of target protein-induced cascade DNA branched amplification reaction and monitoring using citrate-capped AuNPs. (For interpretation of the references to color in this scheme, the reader is referred to the web version of this article.)

At first, the assembled products were corroborated by conducting MetaPhor agarose gel electrophoresis (Fig. 1A). With increasing the concentration of VEGF, the bands corresponding to the assembled products with much lower mobility became distinguishable from lane 2 to lane 3. Additionally, we use Image J to quantitate the brightness intensity of the band of the S1 region (Fig. 1B). In the previous study (Xuan and Hsing, 2014), the position of band 5 (with only the S2 sample) is the same as that of the byproduct sample, so it is difficult to evaluate the amount of the S2 sample. With the increase of VEGF concentration, compared with the same migration position as in lane 1, the S1 region of lane 2 and lane 3 exhibited 47% and 58% intensity decrease, indicating the participation of substrate DNAs in the branched DNA cascade reaction. The hybridization reaction between VEGF and DNA amplification components was further examined via fluorescence measurements (Fig. S2) and quartz crystal microbalance (Fig. S3). With these experiments, it can be concluded that the introduction of VEGF led to the successful formation of DNA dendrimer products. To validate the feasibility of the proposed colorimetric assay, absorption spectra for a VEGF analysis using a series of differential experiment conditions are depicted in Fig. S4. Additionally, we used the ratio of absorbance at 640 and 520 nm (A640/A520) to evaluate the degree of AuNP aggregation (inset of Fig. S4). A higher ratio is associated with red-colored dispersed particles, while a lower ratio is associated with blue-colored aggregates. In the absence of VEGF (Fig. S4A[3]), the absorption band was observed at approximate 520 nm, and the color of the AuNP solution remained red. Additionally, there was a less than 3% increase in the absorption ratio and no color change could be observed when no probe (Fig. S4A[2]) or S1/S2 (Fig. S4A[4]) was used under the same conditions. Nonetheless, the addition of VEGF resulted in the appearance of a broad absorption band from 570 nm to 650 nm followed by the increase of 40% in the absorption ratio (Fig. S4A [1]). This was observed as a change from red to reddish-violet, suggesting the aggregation of AuNPs. Interestingly, the red AuNP solution also exhibited an obvious reddish-violet color change and a 31% enhancement of the absorption ratio (Fig. S4A[5]), which implied that single-stranded DNA (A1/A2) plays an important role in the control of AuNP assembly.

The analytical performance of the NLHCR-based colorimetric aptasensor was characterized under optimal experimental conditions (Fig. S5). Without the introduction of VEGF, there was only one peak (absorption maximum of 520 nm). When the VEGF concentration increased, another broad absorption maximum began to appear at a longer wavelength (Fig. S4B). By analyzing the change in the absorption ratio with respect to VEGF concentration, a linear relationship between the logarithm of the VEGF concentration and ratio shift was observed over a range of 10–200 ng/mL (R^2=0.903) with a limit of detection of 10 ng/mL, which corresponds to 370 pM of VEGF (~27 kDa) (Fig. 1C). To investigate the selectivity of the assay, the absorption ratio change for AuNPs was compared for negatively charged bovine serum albumin (BSA) and positively charged interferon gamma (INF-γ) (Fig. 1D). Based on our results, the increase in the ratio of A640/A520 was negligible for negatively charged BSA. Nevertheless, a slight increase in the spectral ratio with positively charged INF-γ was observed, presumably resulting from the electrostatic interactions between AuNPs and INF-γ proteins.

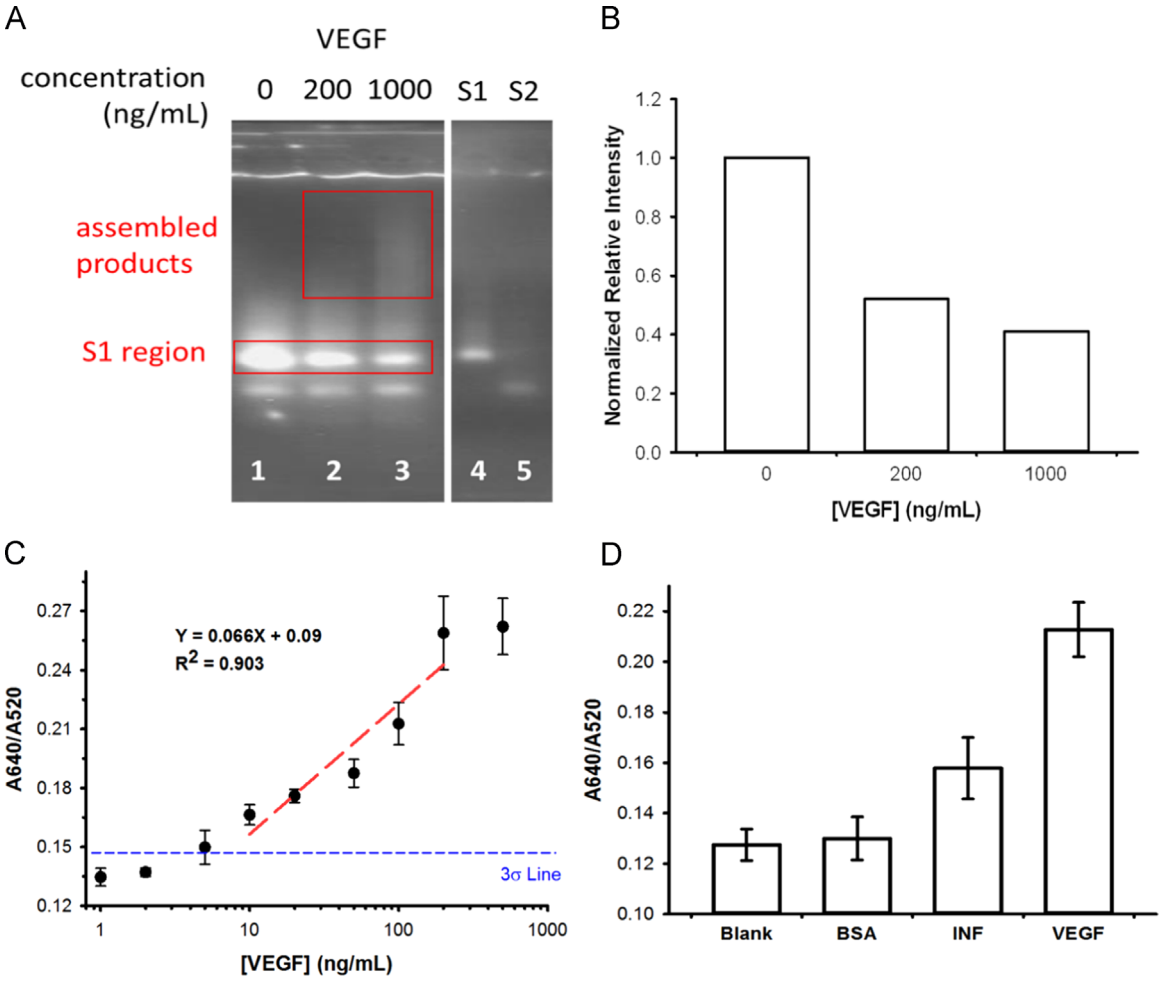

Fig. 1. (A) MetaPhor agarose gel electrophoresis characterization of the formation of the assembled products with the addition of (1) 0 ng/mL, (2) 200 ng/mL, and (3) 1000 ng/mL VEGF. (B) ImageJ software was used to calculate the relative intensity, which was normalized to the S1 region of lane 1. (C) Absorption ratio change in the presence of VEGF at various concentrations. Red line shows linear regression. Final concentrations of S1, S2, A1, A2, and HP are 50, 50, 50, 50, and 200 nM, respectively. (D) Selectivity of the assay toward VEGF. The concentration of VEGF was 100 ng/mL, and the concentration of other proteins was 200 ng/mL. (For interpretation of the references to color in this figure legend, the reader is referred to the web version of this article.)

3.2. Colorimetric assay using DNA sensing probe-stabilized AuNPs

In order to improve the specificity, DNA sensing probes were employed as colorimetric indicators and electrostatic protectors of AuNPs. AuNPs were first treated with DNA sensing probes that were designed to be perfectly complementary to the exposed initiator domains. Fig. 2A depicts the sensing principle. In the presence of target proteins, the branched DNA cascade reaction is initiated, and the dynamic assembly of DNA components is catalyzed to generate dendritic nanostructures. Following the conformational change from simple duplex DNA to the branched DNA nanostructure, exposed initiator domains can hybridize with the sensing probe and induce the aggregation of AuNPs. As depicted in Fig. 2B, in the absence of VEGF, the obtained AuNP solution presents an absorption peak at 520 nm. However, upon the addition of 50 ng/mL VEGF, there was an obvious decrease in the absorbance at 520 nm and increased extinction between 600 and 700 nm, accompanied by a gradual color change from wine red to violet purple. We supposed that the sensing probe bound to the initiator domain of the DNA dendrimer assembled probe; this hybridization event led to the dissociation of sensing probes from AuNP surfaces, and could not protect AuNPs from salt-induced aggregation. To support this explanation, control experiments using random DNA under the same conditions were performed. Clearly, Fig. S6 shows that there was no difference in the absorption band of AuNPs before and after the addition of VEGF. It showed that aggregation only occurs when the sensing probe interacts with the exposed initiator domain in the presence of the added target, indicating the feasibility of this approach.

The sensitivity and dynamic range of the NLHCR biosensor were investigated under the appropriate experimental conditions (Fig. S7). As shown in Fig. 2C, a detection limit of 5 ng/mL (185 pM) was readily accomplished within 50 min. Above this limit, we observed a definite decrease in the absorbance at 520 nm as the target concentration increased and the absorbance ratio showed a good linear correlation in the range of 5 ng/mL (185 pM) to 1000 ng/mL (7.4 nM) in logarithmic scales (Fig. 2D). Compared with the citrate-capped AuNP assay, the present sensing probe-stabilized AuNP assay exhibited a 2-fold lower detection limit and a broader linear range. This sensitivity is also much higher than those of several electrochemical and electric approaches (Lin et al., 2015), surface plasmon resonance (Kang et al., 2008) and colorimetric assays (Shukoor et al., 2012), and is even comparable to that of fluoresce-based biosensors (Nonaka et al., 2013). Although more sensitive approaches based on Exonuclease III amplification followed by fluorescence resonance energy transfer detection have been recently reported (Freeman et al., 2012), our strategy shows distinct advantages. It provides a low limit of detection without

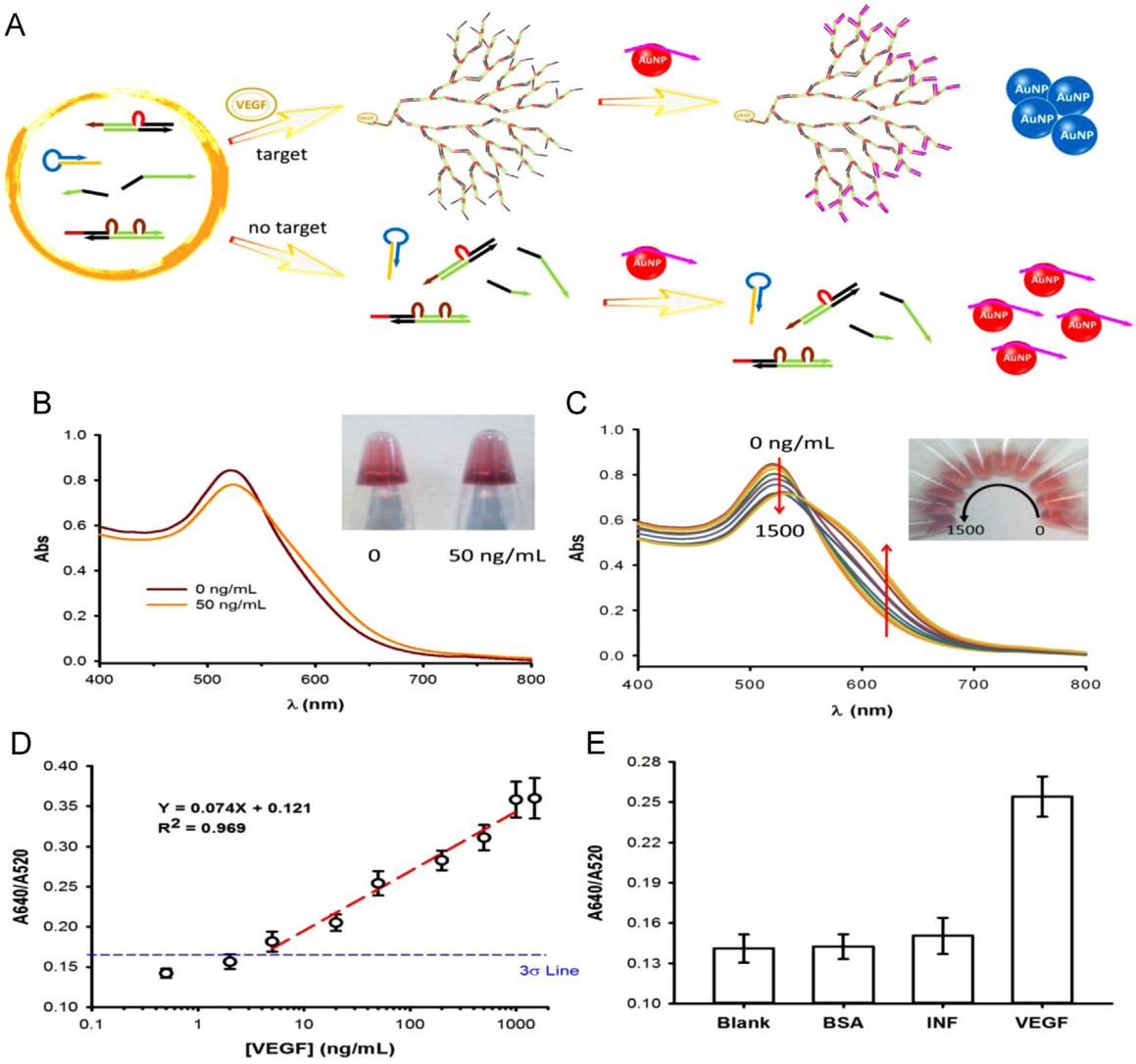

Fig. 2. Colorimetric detection of VEGF using DNA sensing probe-stabilized AuNPs. (A) Principle for VEGF detection. (B) Absorption spectra of AuNPs before and after the addition of VEGF. (B) Absorbance response for different concentrations of VEGF. (C) Absorption ratio change (A640/520) in the presence of VEGF at various concentrations. Red line shows linear regression. Final concentrations of S1, S2, A1, A2, HP, and sensing probe were 50, 50, 50, 50, 200, 300 nM, respectively. (D) Selectivity of the assay toward VEGF. The concentration of VEGF was 50 ng/mL, and the concentration of other proteins was 200 ng/mL.

requiring enzyme amplification or fluorescence conjugation, taking advantage of a novel biosensor. The level of VEGF in healthy adults is as low as 4.5 ng/mL, and concentrations exceeding 12.8 ng/mL are an indicator of colorectal cancer (Dbouk et al., 2007). Therefore, the limit of detection of 5 ng/mL observed in the present assay is sufficient to monitor increased VEGF levels associated with colorectal cancer. We anticipate that the sensitivity can be increased by investigating the concentration of the hairpin aptamer probe, the length of the DNA sensing probe, the incubation time for sensing probe-branch DNA binding, and the diameter of AuNPs; such modifications are in progress and will be reported elsewhere.

The specificity of the developed aptasensor was also evaluated by incubating it with INF-γ and BSA (Fig. 2E). Proteins other than VEGF did not cause any noticeable changes under identical conditions. The nonspecific groups gave an absorption ratio of ~0.15 a.u., which was close to the noise observed for the blank. These results clearly indicate that DNA cascade amplification events were specifically induced by VEGF, demonstrating good selectivity of the strategy. Also, the sensing probe-stabilized AuNP-based method was used to detect VEGF in human serum samples. The results for the clinical samples spiked with various VEGF concentrations are given in Table S2, which were in agreement with a quantitative recovery of less than 25% (Djoba Siawaya et al., 2008), indicating the potential for clinical analysis.

4. Conclusions

In summary, we developed an aptameric amplification assay that combines AuNP colorimetric detection with target-catalyzed branched DNA cascade amplification, and assessed the method using VEGF as an example. The capture probe-based assay had a broad linear range up to 7.4 nM with a low detection limit of 185 pM (corresponding to approximately 3.7 fmole of VEGF molecules in 200 μL of solution). The merits of the assay are that it does not require time-consuming AuNP surface modification and enzymatic amplification steps. Additionally, this assay requires less than an hour for its completion, compared with several hours for HCR-based detection. This nano-plasmonic assay is a potentially versatile sensing strategy for the detection of numerous disease-related biomarkers and other targets of interest.

Acknowledgments

This work was supported by the Ministry of Science and Technology of ROC (102-2218-E-002-014-MY3 and 104-2811-E-002-008), Aim for the Top University Plan of the National Taiwan University (104R104005), and the Mackay Memorial Hospital (104-05, 105-04, and MMH-CT-10408).

Appendix A. Supplementary material

Supplementary data associated with this article can be found in the online version at http://dx.doi.org/10.1016/j.bios.2015.11.051.

References

Chang, C.C., Lin, S., Wei, S.C., Chen, C.Y., Lin, C.W., 2011. Biosens. Bioelectron. 30 (1), 235–240.
Chang, C.C., Chen, C.C., Wei, S.C., Lu, H.H., Liang, Y.H., Lin, C.W., 2012a. Sensors 12 (6), 8319.
Chang, C.C., Lin, S., Lee, C.H., Chuang, T.L., Hsueh, P.R., Lai, H.C., Lin, C.W., 2012b. Biosens. Bioelectron. 37 (1), 68–74.
Chang, C.C., Wei, S.C., Wu, T.H., Lee, C.H., Lin, C.W., 2013. Biosens. Bioelectron. 42, 119–123.
Chang, C.C., Chen, C.P., Lee, C.H., Chen, C.Y., Lin, C.W., 2014a. Chem. Commun. 50, 14443–14446.
Chang, C.C., Chen, C.Y., Zhao, X., Wu, T.H., Wei, S.C., Lin, C.W., 2014b. Analyst 139, 3347–3351.
Dbouk, H.A., Tawil, A., Nasr, F., Kandakarjian, L., Abou-Merhi, R., 2007. Open. Clin. Cancer J. 1, 1–5.
Dirks, R.M., Pierce, N.A., 2004. Proc. Natl. Acad. Sci. USA 101 (43), 15275–15278.
Djoba Siawaya, J.F., Roberts, T., Babb, C., Black, G., Golakai, H.J., Stanley, K., Bapela, N. B., Hoal, E., Parida, S., van Helden, P., Walzl, G., 2008. PLoS One 3 (7), e2535.
Freeman, R., Girsh, J., Fang-ju Jou, A., Ho, J.-aA., Hug, T., Dernedde, J., Willner, I., 2012. Anal. Chem. 84 (14), 6192–6198.
Jiang, Y.S., Bhadra, S., Li, B., Ellington, A.D., 2014. Angew. Chem. Int. Ed. Engl. 53 (7), 1845–1848.
Huang, J., Wu, Y., Chen, Y., Zhu, Z., Yang, X., Yang, C.J., Wang, K., Tan, W., 2011. Angew. Chem. Int. Ed. Engl. 50 (2), 401–404.
Hussain, M.M., Samir, T.M., Azzazy, H.M.E., 2013. Clin. Biochem. 46 (7–8), 633–637.
Jung, C., Ellington, A.D., 2014. Acc. Chem. Res. 47 (6), 1825–1835.
Kang, H., Ryu, S., Hahn, S., Oh, E., Park, J., Kim, K., 2008. Macromol. Res. 16 (2), 182–184.
Kim, Y.S., Chung, J., Song, M.Y., Jurng, J., Kim, B.C., 2014. Biosens. Bioelectron. 54, 195–198.
Li, H., Rothberg, L., 2004. Proc. Natl. Acad. Sci. USA 101 (39), 14036–14039.
Li, J., Macdonald, J., 2015. Biosens. Bioelectron. 64, 196–211.
Lin, X., Chen, Q., Liu, W., Yi, L., Li, H., Wang, Z., Lin, J.M., 2015. Biosens. Bioelectron. 63, 105–111.
Liu, J., 2012. Phys. Chem. Chem. Phys. 14 (30), 10485–10496.
Ma, H., Liu, J., Ali, M.M., Mahmood, M.A.I., Labanieh, L., Lu, M., Iqbal, S.M., Zhang, Q., Zhao, W., Wan, Y., 2015. Chem. Soc. Rev. 44 (5), 1240–1256.
Nonaka, Y., Yoshida, W., Abe, K., Ferri, S., Schulze, H., Bachmann, T.T., Ikebukuro, K., 2013. Anal. Chem. 85, 1132–1137.
Otrock, Z.K., Makarem, J.A., Shamseddine, A.I., 2007. Blood Cells Mol. Dis. 38 (3), 258–268.
Saha, K., Agasti, S.S., Kim, C., Li, X., Rotello, V.M., 2012. Chem. Rev. 112 (5), 2739–2779.
Shawky, S.M., Bald, D., Azzazy, H.M.E., 2010. Clin. Biochem. 43 (13-14), 1163–1168.
Shukoor, M.I., Altman, M.O., Han, D., Bayrac, A.T., Ocsoy, I., Zhu, Z., Tan, W., 2012. ACS Appl. Mater. Interfaces 4 (6), 3007–3011.
Song, W., Zhu, Z., Mao, Y., Zhang, S., 2014. Biosens. Bioelectron. 53, 288–294.
Spiga, F.M., Bonyár, A., Ring, B., Onofri, M., Vinelli, A., Sántha, H., Guiducci, C., Zuccheri, G., 2014. Biosens. Bioelectron. 54, 102–108.
Wang, F., Lu, C.H., Willner, I., 2014. Chem. Rev. 114 (5), 2881–2941.
Wang, X., Jiang, A., Hou, T., Li, H., Li, F., 2015. Biosens. Bioelectron. 70, 324–329.
Xie, S., Chai, Y., Yuan, Y., Bai, L., Yuan, R., 2014. Biosens. Bioelectron. 55, 324–329.
Xuan, F., Hsing, I.M., 2014. J. Am. Chem. Soc. 136 (28), 9810–9813.
Zhang, D.Y., Seelig, G., 2011. Nat. Chem. 3 (2), 103–113.
Zhao, Z., Fan, H., Zhou, G., Bai, H., Liang, H., Wang, R., Zhang, X., Tan, W., 2014. J. Am. Chem. Soc. 136 (32), 11220–11223.